Analytical potential energy surface for the reaction with intermediate complexes NH3 + Cl → NH2 + HCl: Application to the kinetics study

ARTICLE *in* INTERNATIONAL JOURNAL OF QUANTUM CHEMISTRY · APRIL 2012

Impact Factor: 1.43 · DOI: 10.1002/qua.23165

4 AUTHORS, INCLUDING:

Cipriano Rangel
Universidad de Extremadura
27 PUBLICATIONS **321** CITATIONS
SEE PROFILE

Jose C Corchado
Universidad de Extremadura
118 PUBLICATIONS **3,304** CITATIONS
SEE PROFILE

Joaquin Espinosa-Garcia
Universidad de Extremadura
141 PUBLICATIONS **2,191** CITATIONS
SEE PROFILE

Analytical Potential Energy Surface for the Reaction with Intermediate Complexes $NH_3 + Cl \rightarrow NH_2 + HCl$: Application to the Kinetics Study

M. MONGE-PALACIOS, C. RANGEL, J. C. CORCHADO, J. ESPINOSA-GARCÍA

Departamento de Química Física; Universidad de Extremadura, 06071 Badajoz, Spain

Received 22 February 2011; accepted 28 April 2011
Published online 20 June 2011 in Wiley Online Library (wileyonlinelibrary.com).
DOI 10.1002/qua.23165

ABSTRACT: We present for the first time an analytical potential energy surface (PES) for the reaction of hydrogen abstraction from ammonia by a chlorine atom. It has a very complicated shape with various maxima and minima. The functional form used in the development of the PES considered the stretching and bending nuclear motions, and the parameters in the calibration process were fitted to reproduce exclusively high-level ab initio electronic structure calculations obtained at the CCSD(T) = FULL/aug-cc-pVTZ//CCSD(T) = FC/cc-pVTZ single point level. Thus, the surface is completely symmetric with respect to the permutation of the three ammonia hydrogen atoms, and no experimental information is used in the process. The ab initio information used in the fit includes a wide spectrum of properties (equilibrium geometries, relative energies, and vibrational frequencies) of the reactants, products, saddle point, intermediate complexes in the entry and exit channels, points on the reaction path, and points on the reaction swath. By comparison with the reference results, we show that the resulting PES reproduces not only the ab initio data used in the fitting procedure but also other thermochemical and kinetics results computed at the same ab initio level, which were not used in the fit—equilibrium constants, rate constants, and kinetic isotope effects. This represents a severe test for the new surface. As a first application, we perform an extensive kinetics study using variational transition-state theory with semiclassical transmission coefficients over a wide temperature range, 200–2000 K, on this analytical PES. The forward rate constants reproduce the sparse experimental measurements, while the reverse ones reproduce the change of activation energy with temperature reported in another theoretical study, although unfortunately there are no experimental

Correspondence to: J. Espinosa-García; e-mail: joaquin@unex.es

Contract grant sponsor: Junta de Extremadura, Spain.
Contract grant sponsor: Fondo Social Europeo.
Contract grant number: IB10001.

data for comparison. Finally, we analyze the influence of the intermediate complexes and the spin–orbit correction on the kinetics results. In summary, these results indicate that the PES adequately describes this reaction, and the reasonable agreement with experiment lends further confidence to this new surface. © 2011 Wiley Periodicals, Inc. Int J Quantum Chem 112: 1887–1903, 2012

Key words: Cl(2P); potential energy surface; maxima and minima; kinetics study; spin–orbit

1. Introduction

One of the most important bottlenecks in kinetics and dynamics studies of chemical reactivity is the construction of a potential energy surface (PES), which describes the reactive system. For small systems (three or four atoms) with direct mechanisms, PES construction is a relatively mature field, although even today new surfaces are still being developed for atom–diatom systems using very high-level ab initio calculations [1–3]. However, the evolution toward polyatomic systems ($n > 4$ atoms) with direct mechanisms is currently a theoretical and computational challenge, and we have contributed to this field in developing surfaces for five [4–6], six [7–17], and seven [18] atoms. The methodological approach used for these systems was to choose a suitable functional form that correctly describes the stretching and bending movements of the system, which are basically valence bond–molecular mechanics (VB-MM) type surfaces and then to calibrate it against theoretical and/or experimental information. Therefore, in this sense, the surfaces are semiempirical. However, in the last surfaces [6, 9], we avoided this semiempirical character using exclusively high-level ab initio calculations in the calibration process. This represents a methodological alternative to other ways of constructing surfaces in which thousands of geometrical configurations are calculated with high-level electronic structure calculations and then interpolated or fitted to suitable functional forms to obtain the PES. To avoid the difficulties of constructing an analytical form of the PES, the direct dynamics method is increasingly being used in dynamical studies in which the energies and energy derivatives needed to solve the classical trajectory equations are evaluated "on the fly." However, these alternatives give adequate PESs only when ab initio calculations of very high-level are used, and this is still prohibitive for atoms beyond the second row and usually requires a subsequent final refit.

An important challenge in this field was the evolution from symmetrically substituted polyatomic reactions of type CX_4+A, where all the X atoms are equivalent and A is the abstractor atom, to asymmetrically substituted polyatomic reactions of type CWXYZ + A. Using the aforementioned strategy, we developed surfaces for monosubstitutions, H+CH_3Cl, and polysubstitutions, Cl+$CHClF_2$ [19, 20]. Clearly, this involves severe complications in the PES construction process, because now the bonds and angles must be treated independently, but it does make it possible to study different pathways.

We had until now applied this strategy to reactions with direct mechanisms, both with and without barriers in the reaction path. In this work, we propose an extension of this method to reactions with more complicated potentials that can have multiple minima and maxima. As Clary observed recently [21], "Reactions with several maxima and minima in the PES present the severest challenge to calculating and fitting PESs and carrying out quantum dynamics calculations."

To test this new strategy, we shall build the PES for the NH_3 + Cl(^{2}P) hydrogen abstraction reaction,

$$NH_3 + Cl(^2P) \rightarrow CR \rightarrow SP \rightarrow CP \rightarrow NH_2 + HCl \quad (R1)$$

which evolves through a reactant complex (CR) in the entry channel, a saddle point, and a product complex (CP) in the exit channel. This reaction of ammonia with chlorine atoms has been little studied, whether experimentally or theoretically, possibly because its chemistry is very complex with many fast intermediate reactions being involved [22]. To the best of our knowledge, only two kinetics measurements have been reported experimentally. In 1977, using the flash photolysis resonance fluorescence technique, Westenberg and DeHass [23] determined the rate constant at room temperature, $k(298\ K) = 1.23 \times 10^{-13}$ cm^3

molecule^{-1} s^{-1}. Recently, Gao et al. [24], using the time-resolved resonance fluorescence technique, presented the first determination of the temperature dependence in the range 290–570 K for this endothermic reaction. Their fit to the forward rate constant was $k(T) = (1.08 \pm 0.05) \times 10^{-11}$ exp(-2.74 ± 0.04 kcal mol^{-1}/RT) cm^3 molecule^{-1} s^{-1}, with a value of 1.06×10^{-13} cm^3 molecule^{-1} s^{-1} at room temperature, in close agreement with the previous measurement. Theoretically, we know of only four studies [24–27]. Recently [27], we have performed an exhaustive theoretical study of the title reaction using a high ab initio level [CCSD(T)/cc-pVTZ], with the main aim of accurately defining the barrier height and the stability of the intermediate complexes in the entry and exit channels. Moreover, we calculated the reaction path with the "direct dynamics" method [28], which describes a chemical reaction by using ab initio information (energies, gradients, and Hessians) only in the region of configuration space along the reaction path. To obtain kinetics information, we performed variational transition-state theory (VTST) calculations with multidimensional tunneling corrections.

The rest of this communication is organized as follows. In Section 2, high-level electronic structure calculations are outlined, with especial caution taken with respect to the barrier height, the stability of the complexes, and the topology of the reaction path from reactants to products, because these are sensitive parameters in the calibration process. In Section 3, the new PES is constructed and calibrated and is then tested against theoretical electronic structure data in Section 4. Section 5 gives the computational details. The kinetics results using variational transition-state theory with a multidimensional tunneling effect (VTST-MT) are presented in Section 6 and compared with theoretical results and with the sparse experimental kinetics information. Finally, Section 7 gives the conclusions.

2. Electronic Structure Calculations

One of the most difficult energy properties to estimate of a PES is the barrier height. Different laboratories have reported electronic structure calculations for the title reaction using very different levels (correlation energy and basis set) [24–27]. Thus, Kondo et al. [25] performed ab initio calculations using the Gaussian-2 (G2) theory, finding an enthalpy of activation at 0 K, [$\Delta H^{\neq}$(0 K), zero-point corrected barrier height], of 4.75 kcal mol^{-1}. Later, in 2006, Gao et al. [24] constructed the reaction path using the MPWB1K density functional (DFT) method [29], finding $\Delta H^{\neq}(0\ \mathrm{K}) = 2.1$ kcal mol^{-1}, although with the use of different correlation energy levels and basis sets, they found values in the range 1.7–3.1 kcal mol^{-1}, all of which in any case are considerably lower than the value reported by Kondo et al. Xu and Lin [26] performed a computational study of the mechanisms and kinetics of the reaction. The geometries of the stationary points were optimized using the B3LYP DFT method, and their energies were refined with the modified Gaussian-2 (G2M) theory. They obtained $\Delta H^{\neq}(0\ \mathrm{K}) = 4.2$ kcal mol^{-1}, in contrast with the preceding values. Finally, in a previous article [27], we optimized and characterized the stationary point geometrical parameters at the single and double coupled cluster theory level with the inclusion of a perturbational estimate for triple excitations [30], CCSD(T), using the cc-pVTZ basis set [31]—in brief, the CCSD(T)/cc-pVTZ level. We obtained a barrier height of 7.6 kcal mol^{-1}, $\Delta H^{\neq}(0\ \mathrm{K}) = 3.5$ kcal mol^{-1}. In that study we also considered spin–orbit (s–o) coupling, because the chlorine atom has two low-lying fine structure electronic states, $^2P_{1/2}$ and $^2P_{3/2}$, with a separation [32] of $\varepsilon = 882$ cm^{-1} ≈ 2.5 kcal mol^{-1}. A relativistic study was beyond the scope of that work, and the s–o coupling was simulated in our nonrelativistic calculations by adding one-third of the split between the two states, that is, 0.8 kcal mol^{-1} to the barrier height, in which we assumed that the s–o coupling is essentially fully quenched at the saddle point (see below). With this correction, our best estimate of the barrier height was 8.4 kcal mol^{-1}, with an enthalpy of activation at 0 K, $\Delta H^{\neq}$(0 K), equal to 4.3 kcal mol^{-1}, in excellent agreement with the value reported by Xu and Lin [26] who also included the s–o effect in their calculations.

However, it is well known that the classical barrier height is very sensitive to extension of the one-electron basis set and that truncation of the one-electron basis set is the major source of error in most ab initio calculations of molecular energies. In the present work, to obtain the basis set limit, we use Truhlar's infinite basis-set extrapolation method (IB) [33, 34] based on the CCSD(T) level with cc-pVDZ and cc-pVTZ basis sets (correlation-consistent polarized valence double and triple zeta) [31]. This method yields more accurate energies

than those from a straight correlation-consistent polarized sextuple-zeta basis at <1% of the cost [33, 34]. The total energy for the IB method is

$$E_{\infty}^{\text{Total}} = E_{\infty}^{\text{HF}} + E_{\infty}^{\text{corr}} = \frac{3^{\alpha}}{3^{\alpha}-2^{\alpha}}E_3^{\text{HF}} - \frac{2^{\alpha}}{3^{\alpha}-2^{\alpha}}E_2^{\text{HF}} + \frac{3^{\beta}}{3^{\beta}-2^{\beta}}E_3^{\text{corr}} - \frac{2^{\beta}}{3^{\beta}-2^{\beta}}E_2^{\text{corr}} \quad (1)$$

where "corr" is the correlation energy, "HF" is the Hartree–Fock energy, and the subscripts 2 and 3 represent the energies using the double- or triple-zeta bases, respectively. The parameters α and β have values 3.39 and 2.02, respectively. Using the IB extrapolated scheme, one obtains a lower barrier, 8.0 kcal mol^{-1}, that is, 0.4 kcal mol^{-1} lower than the nonextrapolated theoretical value [27], $\Delta H^{\neq}(0\text{ K}) = 3.9$ kcal mol^{-1}.

Recently, Truhlar et al. [35] have used a new database to assess electronic structure methods for barrier heights. They showed that the expensive CCSD(T) = FC/cc-pVTZ level (where FC means frozen core) presents a mean unsigned error (MUE) of 2.86 kcal mol^{-1}, while the correlation of all electrons (FULL) and the use of a larger basis set have a major influence on the description of the barrier. Thus, the CCSD(T) = FULL/aug-cc-pVTZ level used in this study presents a MUE of 0.47 kcal mol^{-1}, comparable with the "best" method found by Truhlar et al. [35]. Using the single point calculation at the CCSD(T) = FULL/aug-cc-pVTZ level, we obtain a barrier height of 6.6 kcal mol^{-1} (s–o included), that is, 1.4 kcal mol^{-1} lower than that obtained with the IB method. This result illustrates the dramatic influence of the electronic correlation and the basis set on the correct description of the barrier. These will be the values used to fit the analytical PES (Section 3).

In our previous work [27], we performed an exhaustive theoretical study of the intermediate complexes in the entry and exit channels. This information will not be repeated in full here, but in brief, if one neglects the s–o coupling then the electronic ^{2}P ground-state of the chlorine atom is triply degenerate. Interaction with the NH_3 molecule removes this degeneracy, giving rise in general to three orthogonal states. In the C_s symmetry, the states are 1 ^{2}A′, 2 ^{2}A′, and 1 ^{2}A″. The first corresponds to the singly occupied 3p orbital of the chlorine atom pointing directly toward the nitrogen atom of the NH_3 molecule, whereas for the 2 ^{2}A′ and 1 ^{2}A″ states, the singly occupied 3p orbital is orthogonal to the Cl···N axis. For the hydrogen abstraction reaction studied in the present work, two intermediate complexes were located in the entry channel and characterized close to the reactants as minima (Fig. 1). One of them presents a typical Cl···H—N bond, termed CR1, with the doubly occupied chlorine 3p orbital pointing toward the N atom being energetically favored (^{2}A′ symmetry). The second presents a two-center/three-electron Cl ∴ N bond, termed CR3, now with the singly occupied chlorine 3p orbital pointing toward the N atom being energetically favored (^{2}A′ symmetry). In the exit channel, a hydrogen bond complex (CP) was located and characterized as a true minimum (Fig. 1). At the CCSD(T)/cc-pVTZ level, the CR1 is weakly stabilized with respect to the reactants, −0.7 kcal mol^{-1}, $\Delta H(0\text{ K}) = -0.5$ kcal mol^{-1}, while the CR3 is strongly stabilized with respect to the reactants, −5.4 kcal mol^{-1}, $\Delta H(0\text{ K}) = -4.6$ kcal mol^{-1}. At the highest level, we used CCSD(T)=FULL/aug-cc-pVTZ//CCSD(T)=FC/cc-pVTZ, while the CR1 is slightly modified, $\Delta E = -1.0$ kcal mol^{-1}, the CR3 is strongly stabilized with respect to the reactants, $\Delta E = -7.2$ kcal mol^{-1}. Therefore, it is expected that the hydrogen abstraction reaction will evolve preferentially at the most stabilized complex, CR3. Indeed, our calculations show that, depending on the orientation of the two reactants, they can follow any of the downhill paths leading to either of the two complexes. Afterward, low-barrier reactions transform CR3 into CR1, which is the complex that one gets when following the saddle point downhill in the direction to

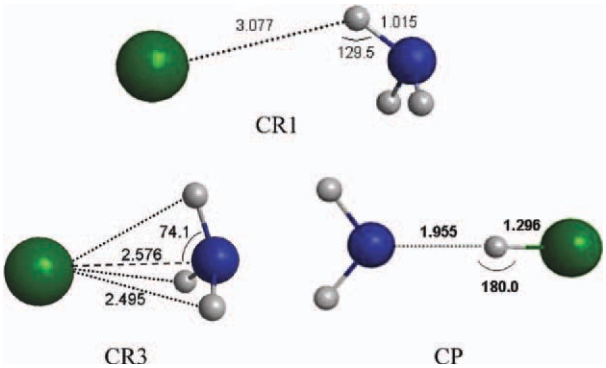

FIGURE 1. Geometric parameters (distances in Å and angles in degrees) of intermediate complexes at the CCSD(T) = FC/cc-pVTZ level. [Color figure can be viewed in the online issue, which is available at wileyonlinelibrary.com.]

reactants. The system then evolves toward the products by overcoming the barrier to reaction. Therefore, due to the greater stability of the CR3 complex, one can safely assume that it plays a more important role in the system's reactivity and dynamics than the CR1 complex.

The CR3 complex has been previously reported only by Xu and Lin [26], although at the lower B3LYP DFT level. Those workers found a similar geometry, with an enthalpy of reaction at 0 K of -3.6 kcal mol^{-1} at the "single point" G2M//B3LYP level. The CP is also strongly stabilized, -7.1 kcal mol^{-1}, $\Delta H(0\ \mathrm{K}) = -5.3$ kcal mol^{-1} (s–o not included), with respect to the products. Doubtless, these wells in the entry and exit channels will influence the dynamics of the reaction, but they will make the construction of the analytical PES very difficult.

Note that in the entry well the s–o coupling was not included, because we assume that this interaction stabilizes both the Cl(^{2}P) atom and the Cl-molecular complex, while in the exit channel the s–o is included, because it is essentially fully quenched at the CP complex. A relativistic study of this polyatomic reaction is very difficult and is beyond of the scope of the present work. However, to test the validity of the assumptions of the s–o coupling along the reaction path, entry and exit valleys, and saddle point, we made some calculations following a very qualitative approach. Based on a simple CASSCF wavefunction with five electrons and six orbitals, the s–o coupling was calculated as implemented in GAUSSIAN 03 [36]. Taking into account for comparison that the s–o coupling is one-third the chlorine atomic s–o splitting [32], that is, 294 cm^{-1}, we computed an s–o coupling of 254 cm^{-1} for the chlorine atom, in close agreement with the experimental value [32], which lends confidence to the very simple approach used. For the reactant complex CR3, we obtained a value of 247 cm^{-1}, and for the saddle point, a value of 16 cm^{-1}, confirming that, as indicated above, the quenching is very small in the reactant complex, while at the saddle point the s–o coupling is practically quenched.

Finally, for the sake of clarity, Figure 2 shows schematically the variations in potential energy along the hydrogen abstraction reaction path studied in this work.

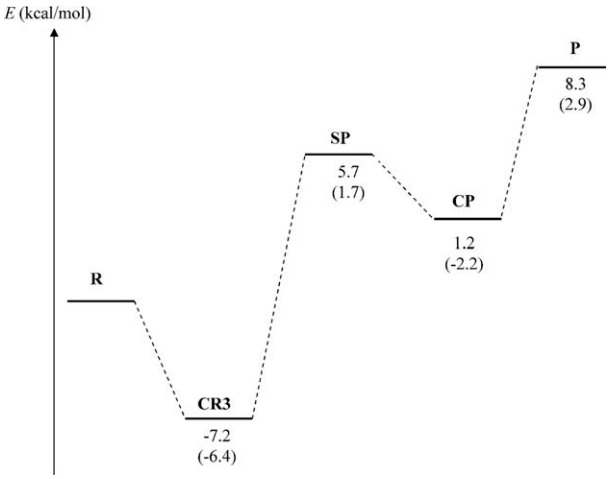

FIGURE 2. Schematic profile of the nonrelativistic potential energy surface along the reaction path, where spin-orbit interactions are not included. Energies at the CCSD(T) = FULL/aug-cc-pVTZ//CCSD(T) = FC/cc-pVTZ single point level, with respect to the reactants, Cl + NH_3. The first entry corresponds to the classical potential energy, and the second entry to the changes of enthalpy at 0 K, ΔH(0 K). Note that ΔH(0 K) in the saddle point corresponds to the enthalpy of activation at 0 K.

3. Analytical PES Function and Fitting Procedure

The analytical PES function we use is based on our PES-NH4 surface [6] describing the similar NH_3 + H hydrogen abstraction reaction. This is basically a VB-MM surface, given by the sum of two terms: a valence bond stretching potential, V_{stretch}, and a molecular mechanics term, the harmonic bending term, V_{harm},

$$V = V_{\mathrm{stretch}} + V_{\mathrm{harm}} \tag{2}$$

The stretching potential is the sum of three London–Eyring–Polanyi (LEP) terms [37], each one corresponding to a permutation of the three ammonia hydrogens,

$$V_{\mathrm{stretch}} = \sum_{i=1}^{3} V_3(R_{\mathrm{NH_i}}, R_{\mathrm{NCl}}, R_{\mathrm{H_iCl}}) \tag{3}$$

where R is the distance between the two subscript atoms and H_i stands for one of the three ammonia hydrogens, and where there are 12 fitting parameters, four for each of the three kinds of bond,

R_{NH_i}, R_{NCl}, and R_{H_iCl}. In particular, these are the singlet and triplet dissociation energies, D^1_{XY} and D^3_{XY}, the equilibrium bond distance, R^e_{XY}, and the Morse parameter, α_{XY}, which is allowed to relax from ammonia to the amidogen radical using a switching function that depends on two additional parameters, a and b. Therefore, 14 parameters are required to describe the stretching potential.

One of the problems with this functional [6] was that the equilibrium N—H_i distances for the reactants, saddle point, and products are the same, leading to a very rigid PES-NH4. Based on a recent article of Truhlar et al. [38] on the H + C_2H_6 reaction, a modification is included to endow the new surface with greater flexibility in this article. The reference N—H_i bond distance is transformed smoothly from reactant to product using the equation

$$r^o_{NH} = P_1 r_{NH,Ro} + (1 - P_1) r^o_{NH,P} \tag{4}$$

where P_1 is

$$P_1 = \prod_{i=1}^{3} T_1(r_{NH_i}) \tag{5}$$

which is symmetric with respect to all three hydrogen atoms and goes to zero as one of the hydrogen atoms is abstracted, and T_1 is a geometry-dependent switching function given by

$$T_1(r_{NH}) = 1 - \tan h[w_1(r_{NH} - w_2)] \tag{6}$$

where w_1 and w_2 are adjustable parameters. Therefore, this adds two new parameters (total 16 parameters) to describe the stretching potential.

The V_{harm} term is the sum of three harmonic terms, one for each bond angle in ammonia,

$$V_{harm} = \frac{1}{2} \sum_{i=1}^{3} \sum_{j=i+1}^{2} k^0_{ij} k_i k_j \left(\theta_{ij} - \theta^0_{ij}\right)^2 \tag{7}$$

where k^0_{ij} and k_i are force constants, and θ^0_{ij} are the reference angles. All these magnitudes are allowed to evolve from their value in ammonia to their value in the amidogen radical by means of switching functions. In total, 16 parameters need to be fitted for the calibration of the V_{harm} potential.

The new surface, PES-2010, is symmetric with respect to the permutation of the three equivalent ammonia hydrogens, a feature especially important in dynamics calculations, and depends on 32 parameters, which give great flexibility while keeping the VB-MM functional form physically intuitive.

Having selected the functional form, the 32 parameters describing the new PES-2010 are fitted by using as input information exclusively high-level ab initio calculations at the CCSD(T) = FULL/aug-cc-pVTZ//CCSD(T) = FC/cc-pVTZ single point level, describing all the stationary points and the reaction path and reaction swath. This process has been described in detail elsewhere [8, 13, 16], although for direct mechanisms, but we shall summarize the process here. It consists of four steps. In the first step, we change the parameters of the PES related to the geometry, energy, and vibrational properties of the reactants and products, so that the geometries, heat of reaction, and vibrational frequencies agree with the available theoretical data. In the second step, we refit some parameters to reproduce the characteristics of the quantum mechanically calculated saddle point, in particular, the geometry, barrier height, and vibrational frequencies. In the third step, especial caution is taken respecting the location and characterization of the intermediate complexes in the entry and exit channels, CR and CP, respectively. This greatly complicates the calibration process relative to the method applied in direct mechanisms and represents a major challenge in the calculation and fitting of PESs of this type. Finally, in step four of the calibration, we refit some parameters of the analytical PES to reproduce the topology of the reaction, from reactants to products. This calibration process is thus a far from trivial task and is time consuming because it is an iterative process in which the steps 1–4 must be repeated until convergence of all the ab initio information used in the fit. Figure 3 shows a three-dimensional representation and contour plot of the new PES using the fitted parameters of the final functional form. One notes the presence of the two minima in the entrance and exit channels.

4. Test of Consistency of the New PES: Comparison with Ab Initio Calculations

One way to measure the quality of the fit and of the analytical form is to analyze to what extent the reference information used for the fit, computed at the CCSD(T) = FULL/aug-cc-pVTZ single point level, can be reproduced.

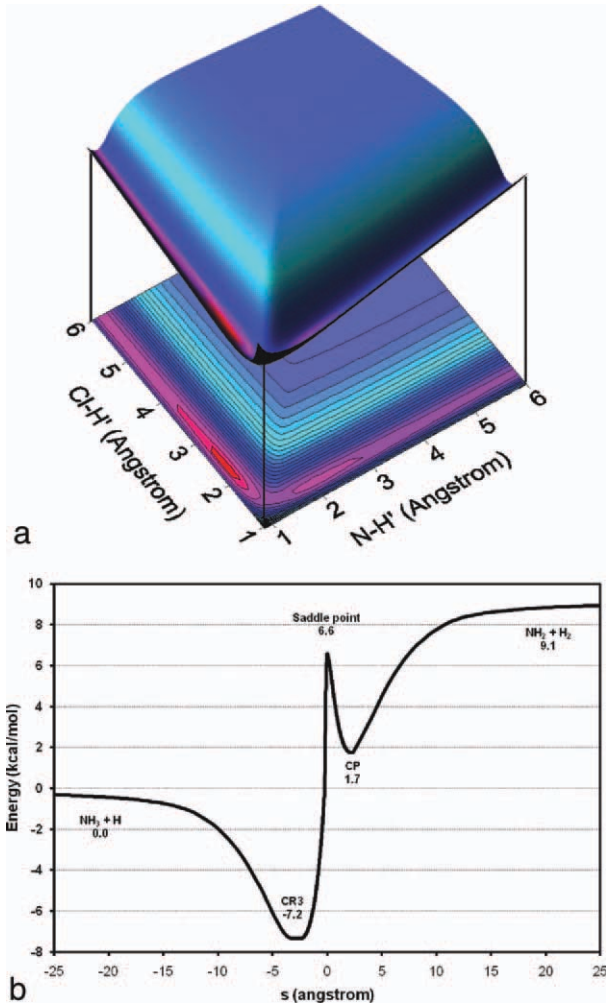

FIGURE 3. (a) Three-dimensional representation of the PES and contour plots of the gas-phase NH_3 + Cl reaction. (b) Two-dimensional plot of the energy along the reaction path for the NH_3 + Cl abstraction channel. [Color figure can be viewed in the online issue, which is available at wileyonlinelibrary.com.]

Tables I and II list the values of the geometries, vibrational frequencies, and energies at the stationary points—reactants, products, and saddle point in Table I, and intermediate complexes in Table II. In general, the agreement between the PES and ab initio values is reasonable, with the most significant differences being the N—H′—Cl bend angle at the saddle point. Although the ab initio calculations give a nonlinear angle, 152.1°, the PES gives a collinear approach, which is the expected behavior of the LEP-type (London–Eyring–Polanyi) function used to describe the stretching term in the potential, Eq. (3). A priori, one would think that it might be possible to use LEP-type surfaces to describe the kinetics and dynamics of systems with noncollinear reaction paths. Two of our group's previous articles [39, 40] analyzed this possibility, using the atom–diatom Cl + HCl and the polyatomic $O(^3P)$ + NH_3 reactions as models, which have a "bent" structure of the saddle points with ab initio calculations, 161.4° and 159.5°, respectively. These studies showed that the collinear LEP-type surfaces and the ab initio "bent" surfaces indeed present similar kinetics and dynamics behavior. This capability of the LEP-type surfaces to reproduce the kinetics and dynamics of polyatomic systems with noncollinear reaction paths is encouraging and represents a great saving in computation time.

With respect to the reaction enthalpy at 0 K, $\Delta H_R(0\ K)$, the PES-2010 value reproduces the ab initio reference, with a difference of 0.2 kcal mol^{-1}. Moreover, the PES enthalpy, 3.9 kcal mol^{-1}, is close to the experimental value, 3.7 ± 0.6 kcal mol^{-1} (see Section 6.2 for more detailed discussions of this value).

The two wells along the reaction path are also reasonably well described, although the differences between the ab initio and PES results are larger than for the other stationary points. Because of the mathematical form of the PES as well as the calibration process, we were unable to get a better description of these complexes without worsening the fit of the saddle point area. As the saddle point area is much more relevant to an adequate description of the reaction kinetics and dynamics, and the characteristics of these rather floppy wells are strongly dependent on the level of calculation, we did not pursue any further refinement in the description of these wells.

Figure 4 plots energy changes along the reaction path. With respect to the reference ab initio single point level, CCSD(T) = FULL/aug-cc-pVTZ, the energy changes along the reaction path are reasonably well described, with the largest differences being about 1.5 kcal mol^{-1} on the reactant side of the reaction path, making the downhill path from the saddle point to the reactant complex less steep than in ab initio calculations. In a different reaction, we would expect this discrepancy to have a significant effect on the kinetics of the reaction that takes place through quantum-mechanical tunneling. However, as we shall show below, tunneling can be neglected in this reaction, and one can expect that the flatter reaction path will have little effect on the reactivity.

TABLE I

Properties of the reactants, products, and saddle point.[a]

Parameter	Geometry		Frequency		ΔV		ΔH (0K)	
	PES	Ab initio[b]	PES	Ab initio	PES	Ab initio	PES	Ab initio
$NH_3(C_{3v})$.								
R(N—H)	1.014	1.014	3636	3600				
<HNH	109.0	105.6	3639	3600				
			3450	3473				
			1724	1687				
			1724	1687				
			1174	1108				
HCl								
R(Cl—H)	1.277	1.277	3026	3001				
NH_2								
R(N—H)	1.027	1.025	3545	3458	9.2	9.1	3.9	3.7
<HNH	103.4	102.2	3493	3366				
			1550	1558				
Saddle point								
R(N—H)	1.029	1.023	3352	3526	6.6	6.6	2.2	2.5
R(N—H′)	1.288	1.337	3257	3420				
R(Cl—H′)	1.364	1.435	1772	1565				
Dihedral	180.0	152.1	1181	1172				
			972	1076				
			716	690				
			549	458				
			480	404				
			1003 *i*	1021 *i*				

[a] Distances in Å, angles in degrees, relative energies in kcal mol^{-1}, and frequencies in cm^{-1}.
[b] Calculations at the CCSD(T) = FULL/aug-cc-pVTZ//CCSD(T)=FC/cc-pVTZ single-point level.

Figure 5 shows the variation of the energy as a function of the N—H′—Cl angle, keeping the remaining parameters in the saddle point geometry at their reference levels. The fitted PES reproduces the ab initio information over the wide range of angles 90–270°. Note that there is a slight deviation in the location of the minimum of this curve, with the fitted PES having its minimum at 180°.

Finally, contour plots for the reference ab initio and the fitted PES are shown in Figure 6. The fitted surface reproduces reasonably well the reaction path, reaction valley, and reaction swath from the ab initio information. This behavior is especially interesting for the following kinetics and dynamics studies.

5. Computational Details

With the new PES-2010 surface, the reaction path was calculated starting from the saddle point geometry and moving downhill to both reactants and products in mass-weighted Cartesian coordinates using Page and McIver's method [41], obtaining the minimum energy path, MEP [42]. Along the MEP, we calculated vibrational frequencies after having projected out the motion along the reaction path using curvilinear redundant internal coordinates [43, 44], which are a nonlinear function of Cartesian coordinates, and they avoid unphysical imaginary values of the vibrfational frequencies over a wide range of the reaction coordiante. With this information, we calculated the respective ground-state vibrationally adiabatic potential curve

$$V_a^G(s) = V_{MEP}(s) + \varepsilon_{int}^G(s) \quad (8)$$

where $V_{MEP}(s)$ is the classical energy along the MEP with its energy zero at the reactants, and $\varepsilon_{int}{}^G(s)$ is the zero-point energy at s. Rate constants were estimated using canonical variational transition-state theory (CVT) [45, 46]. The rotational

TABLE II

Properties of the reactant and product complexes.[a]

	Geometry		Frequency		ΔV		ΔH (0 K)	
Parameter	PES	Ab initio[b]	PES	Ab initio	PES	Ab initio	PES	Ab initio
Reactant complex, CR3.								
R(N—H)	1.017	1.010	3564	3678	−7.2	−7.2	−7.3	−6.4
<HNH	109.0	113.0	3564	3678				
			3373	3506				
			1720	1618				
			1720	1618				
			1158	704				
			126	344				
			46	338				
			46	240				
Product complex, CP								
R(N—H)	1.028	1.027	3462	3495	1.7	2.0	−3.4	−1.6
R(N—H′)	2.069	1.955	3400	3396				
R(Cl—H′)	1.279	1.296	3010	2746				
			1539	1543				
			143	572				
			70	555				
			70	212				
			30	160				
			30	146				

[a] Distances in Å, angles in degrees, relative energies in kcal mol^{-1}, and frequencies in cm^{-1}.
[b] Calculations at the CCSD(T)=FULL/aug-cc-pVTZ//CCSD(T)=FC/cc-pVTZ single-point level.

partition functions were calculated classically. The rotational symmetry number has been set to unity, because we consider the symemtry factor in the expression of the rate constant, which represents the reaction path multiplicity, that is, the number of equivalent reaction paths from reactants to products. For the forward reaction this factor is 3, and for the reverse, 2. By calculating the electron

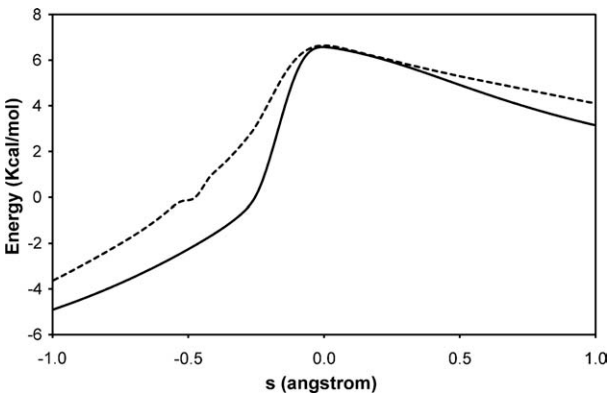

FIGURE 4. Classical potential energy as a function of the reaction coordinate (s) for the hydrogen abstraction reaction between ammonia and chlorine atom. The curves are PES (solid line) and CCSD(T) = FC/cc-pVTZ level (dotted line).

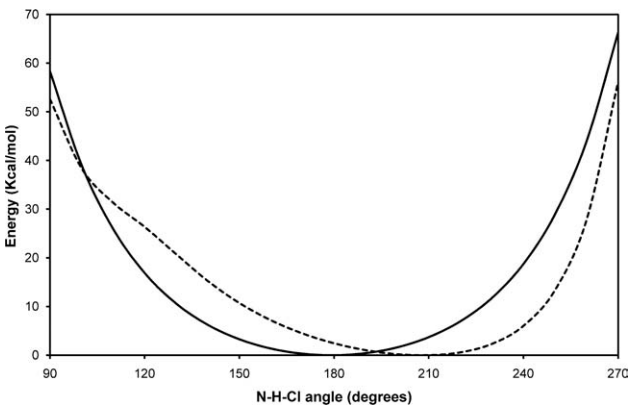

FIGURE 5. Variation of the energy of the saddle point in function of the N—H—Cl angle, from linear to 90° in both toward and from the nitrogen lone pair (keeping the remaining parameters at the saddle point geometry at the reference level). Dotted line: CCSD(T) = FC/cc-pVTZ energies. Solid line: PES energies.

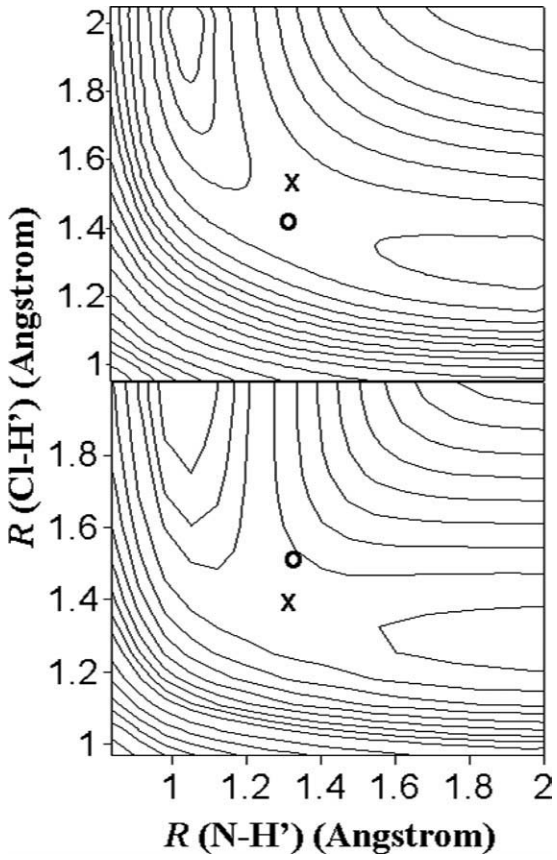

FIGURE 6. Contour plots of the analytical PES (upper panel) and CCSD(T)=FC/cc-pVTZ surface (lower panel) in the proximity of the saddle point. The symbol "X" indicates the location of the CCSD(T) = FC/cc-pVTZ saddle point, while the symbol "0" is the saddle point in the analytical PES.

partition functions, we included the $^2P_{1/2}$ excited state of Cl (with an excitation energy [32] of $\varepsilon = 882$ $cm^{-1} \approx 2.5$ kcal mol^{-1}) in the reactant electronic partition function,

$$Q_e = 4 + 2\ \exp(-\varepsilon/k_B T) \tag{9}$$

assuming that the electronic partition function of the transition state is 2, that is, it is assumed that the s–o effect is fully quenched in this zone. Quantum effects in motions orthogonal to the reaction path were included by using quantum-mechanical vibrational partition functions in the harmonic approximation, and those in the motion along the reaction path by using the microcanonical optimized multidimensional tunneling (μOMT) approach [47] in which, at each total energy, the larger of the small-curvature (SCT) and large-curvature (LCT) tunneling probabilities is taken as the best estimate. We used the centrifugal-dominant SCT [48] and version-4 LCT [49] methods.

A better way to compute tunneling is to optimize the angle between the reaction path and the tunneling path so that the tunneling probability is the highest or the imaginary action is the least. This angle is zero in the zero-curvature tunneling (ZCT) case and 90° in the LCT case. In short, this is least-action tunneling (LAT) [50]. This last method is the most accurate, but it has only very recently been extended to polyatomic reactions [51]. Instead, the microcanonically optimized multidimensional tunneling, μOMT, method represents a rough approximation to LAT. Note that while in LAT there is a consistent way of treating all the tunneling paths, in the μOMT method the approximations used to compute SCT and LCT tunneling probabilities are totally different. In this study, however, with an endothermic reaction where the $V_a^G(s)$ curve evolves without a barrier, the tunneling factor is unity at all temperatures, and therefore, SCT, LCT, and LAT agree.

All kinetics calculations were performed using the general polyatomic rate constant code POLYRATE [47], in which the rotational partition functions are calculated classically.

6. Results and Discussion

As a first application of the new PES, we shall present the kinetics results using variational transition state theory. First, we compare the PES rate constants with the values obtained at the ab initio level (which represents a new test of the accuracy of the surface), and second, we compare the PES rate constants with the sparse available experimental values.

6.1. COMPARISON WITH AB INITIO CALCULATIONS

As was just shown, despite some small differences, the new PES accurately mimics the CCSD(T) = FULL/aug-cc-pVTZ surface, with two main advantages: the computational cost is immensely lower, and the PES gives, in addition to the energies, the analytical first derivatives of the energy, that is, the analytical gradients. Therefore, it is interesting now to test whether the kinetics of this system are also described with great accuracy, bearing in mind that no kinetics

TABLE III

Rate and equilibrium constants.[a]

	K_f (NH_3 + Cl)		K_r (NH_2 + HCl)		K_{eq}	
T(K)	PES	Ab initio	PES	Ab initio	PES	Ab initio
250	4.7E-14	6.4E-14	2.0E-11	2.2E-11	2.4E-3	2.9E-3
298	1.2E-13	1.5E-13	1.2E-11	1.3E-11	1.0E-2	1.1E-2
300	1.2E-13	1.6E-13	1.2E-11	1.3E-11	1.0E-2	1.2E-2
500	9.1E-13	1.2E-12	4.2E-12	5.2E-12	2.2E-1	2.4E-1
800	3.9E-12	5.7E-12	3.1E-12	4.3E-12	1.3	1.3
1000	7.3E-12	1.1E-11	3.2E-12	4.7E-12	2.3	2.3
1500	2.1E-11	3.2E-11	4.6E-12	7.2E-12	4.6	4.5
2000	4.3E-11	6.7E-11	6.9E-12	1.1E-11	6.3	6.1

[a] CVT/SCT rate constants in cm^3 $molecule^{-1}$ s^{-1}. Equilibrium constants are dimensionless. 4.7E-14 means 4.7×10^{-14}. In this case, SCT = 1 at all temperatures.

properties were included in the fit. As kinetics calculations are affordable (although very time consuming) at the CCSD(T) = FULL/aug-cc-pVTZ//CCSD(T) = FC/cc-pVTZ single point level, we carried them out using both the new PES and the ab initio level to gauge the accuracy of the new PES. Table III lists the rate constants for the forward and reverse reactions, as well as the equilibrium constants. Table IV lists some kinetic isotope effects (KIE) computed using both the analytical and the ab initio surfaces.

It is necessary to give some brief details of the KIE calculations. These calculations were performed by recomputing all the reaction paths and rates and taking into account all the possible channels for each isotopic substitution. In the ab initio case, however, recomputing the reaction paths involved enormous effort (for instance, for the title reaction, the calculation of each reaction path at the ab initio level took roughly one year of CPU time on a single-processor Pentium IV computer). Therefore, a single reaction path approach was used [52], because our tests showed that the KIEs computed using this approach with our PES are typically within 10% of the full KIE calculation. This represents an additional advantage of the analytical PES, because the KIE calculations are straightforward and involve very little computational cost.

From the analysis of the rates and the KIEs, we can conclude that the analytical PES reproduces the kinetics results obtained at the ab initio reference level reasonably well.

Finally, it is necessary to note that the ab initio rate constant values in the present work are different from those reported in our previous article [27]. This difference has two causes: first, here we use a more complete ab initio level (see Section 2), which lowers the barrier height by 1.9 kcal mol^{-1}; and second, because in the "direct dynamics" method used in the previous article [27], it was necessary to calculate the energy, gradient, and Hessian at a number of points along the MEP. One might reasonably suppose that the greater the number of points, the better the description of the reaction path. Obviously, if the level of calculation is modest and/or the reaction is symmetric, calculation at every gradient stepsize is both desirable and possible along the entire MEP. However, we are interested in the case of a high level of calculation and large molecular systems, where calculation for every gradient stepsize would be prohibitive. In our previous article,

TABLE IV

Selected KIEs computed using the PES and ab initio rate constants.[a]

	KIE (ND_3 + Cl)		KIE (ND_2H + Cl)	
T (K)	PES	Ab initio	PES	Ab initio
300	9.2	12.3	6.9	5.2
500	4.0	4.5	4.9	4.0
1000	1.9	2.2	4.0	3.5
1500	1.5	1.7	3.6	3.2
2000	1.4	1.6	3.6	3.2

[a] KIEs are defined as the rate for the perprotio reaction over the overall rate for the reaction given in parentheses (CVT/SCT rate constants).

TABLE V

Forward rate constants (cm^3 $molecule^{-1}$ s^{-1}) of the NH_3 + Cl reaction.

T (K)	CVT/LAT[a]	G[b]	G[c]	XL[d]
250	4.7E-14[e]		8.4E-14	4.2E-14
298	1.2E-13		2.5E-13	1.0E-13
300	1.2E-13	1.1E-13	2.6E-13	1.0E-13
350	2.4E-13	2.1E-13	5.9E-13	2.2E-13
400	4.1E-13	3.4E-13	1.1E-12	4.0E-13
500	9.1E-13	6.8E-13	2.7E-12	9.9E-13
600	1.7E-12		4.8E-12	2.0E-12
700	2.7E-12		7.4E-12	3.4E-12
1000	7.3E-12			
1500	2.1E-11			
2000	4.3E-11			

[a] This work, using the PES-2010 surface, considering the s–o coupling and LAT = 1.
[b] Experimental values, from Ref. [24], in the temperature range 290–570 K.
[c] Theoretical values at the MPWB1K DFT model from Ref. [24], in the range 250–750 K.
[d] Theoretical values at the G2M//B3LYP level from Ref. [26].
[e] 4.7E-14 means 4.7×10^{-14}.

due to the high ab initio level used, CCSD(T)/cc-pVTZ, the Hessian calculations were performed only at a reduced number of points along the MEP, with the first points calculated from the saddle point being widely spaced. However, studying a similar reaction [53], we demonstrated the major and indeed definitive influence of this factor on the final rate constants, especially on the tunneling factor: in particular, as the number of points is reduced, the description of the MEP worsens, the barrier narrows, and the tunneling effect rises considerably. For instance, for the NH_3 + H reaction, the tunneling effect increases by a factor of 160 when the number of points calculated is decreased by a factor of two. To correct this effect and to improve the results of our previous work on the title reaction [27], we here performed more extensive calculations of the Hessians close to the saddle point. These are the results listed in Tables III and IV.

6.2. COMPARISON WITH EXPERIMENT

Table V lists the variational CVT/LAT forward rate constants in the temperature range 250–2000 K obtained with the PES-2010 surface, together with experimental [24] and theoretical [24, 26] rate constants for comparison, and Figure 7 shows the corresponding Arrhenius plots. For the comparison with experiment, we use the data of Gao et al. [24] who performed direct measurements recommending the three-parameter expression $k(T) = (1.08 \pm 0.05) \times 10^{-11} \cdot \exp(-2.74 \pm 0.04 \text{ kcal mol}^{-1}/\text{RT})$ cm^3 $molecule^{-1}$ s^{-1}, over the temperature range 290–570 K. The kinetics results with the PES-2010 surface reproduce the experimental measurements over the whole, although limited, temperature range. This agreement is encouraging because, as was mentioned above, no experimental kinetics information was used in the fitting procedure.

Finally, the phenomenological activation energy computed as local slopes of the Arrhenius plot for this reaction is 3.1 kcal mol^{-1}, very close to the experimental value, 2.74 ± 0.04 kcal mol^{-1} [24] in the common temperature range, 290–570 K.

An issue of great importance and active current interest in reactions with free halogen atoms is the role of s–o coupling in the reactivity, because it can reshape the PES, thus complicating the dynamical picture of the reaction [54–58]. The chlorine atom has two low-lying fine structure electronic states, $^2P_{1/2}$ and $^2P_{3/2}$, with a separation of $\varepsilon = 882$ $cm^{-1} \approx 2.5$ kcal mol^{-1} [32]. A priori, this large energy separation would lead one to expect that the reaction with RH molecules could evolve on an adiabatic surface, connecting the s–o ground state, $^2P_{3/2}$, with the products, the contribution of the chlorine excited state, $^2P_{1/2}$, being

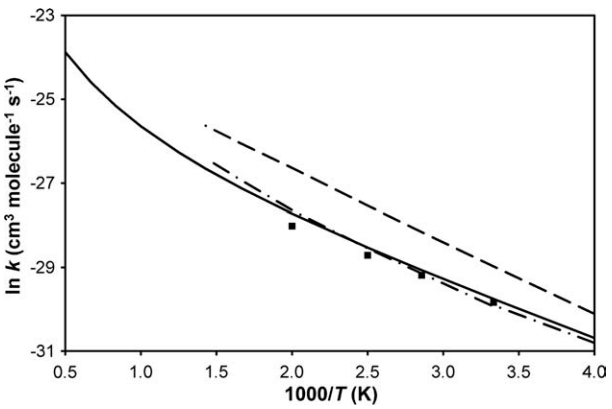

FIGURE 7. Arrhenius plots of ln k (cm^3 $molecule^{-1}$ s^{-1}) for the forward thermal rate constants against the reciprocal of temperature (K) in the range 250–2000 K. Solid line: PES-2010; dashed line: theoretical values from Ref. [24]; dotted-dashed line: theoretical values from Ref. [26], solid squares: experimental values from Ref. [24].

TABLE VI

Equilibrium constants for the NH_3 + Cl → NH_2 + ClH reaction, and reverse rate constants.[a]

	K_{eq}			k_{rev}	
T (K)	PES-2010[b]	G[c]	JANAF [32]	PES-2010[b]	G[d]
298	0.010	0.011	0.002	1.2E-11	2.3E-11
300	0.010	0.011	0.002	1.2E-11	2.3E-11
400	0.068	0.074	0.019	5.9E-12	1.5E-11
500	0.220	0.220	0.077	4.2E-12	1.2E-11
600	0.477	0.470	0.19	3.5E-12	1.0E-11
800	1.267	1.180	0.620	3.1E-12	8.8E-12
1000	2.250	2.055	1.200	3.2E-12	9.2E-12
1500	4.606	4.260	2.740	4.6E-12	1.3E-11
2000	6.252	6.110	3.910	6.9E-11	1.7E-11

[a] In cm^3 $molecule^{-1}$ s^{-1}.
[b] This work, CVT/LAT.
[c] Ref. [24], using the expression $k_{eq} = 27.3\ T^{-0.049}$ exp(−2248/T) over 200–2000 K.
[d] Ref. [24], theoretical values read directly from its Figure 5. In the temperature range 250–750 K, those authors proposed the expression $k_{-1} = 4.08.10^{-13}\ T^{0.343}$ exp (+622/T).

practically negligible according to the Born–Oppenheimer (BO) approximation.

However, recently a controversy has arisen on this point. Liu et al. [59–61] demonstrated experimentally the opposite for the Cl + H_2 reaction, that is, the excited chlorine atom (Cl*) is more reactive to H_2 than the ground-state chlorine (Cl) by a factor of at least ≈ 6, and in any case, even taking into account experimental error bars, the authors were confident about the reactivity relation, Cl* > Cl, which could have a significant effect on the temperature dependence of the thermal rate constants. The authors interpreted this surprising result by postulating a nonadiabatic transition (breakdown of the BO approximation) from the excited Cl* to the ground-state Cl surface, by either electrostatic or s–o coupling in the entrance channel. This experimental study initiated a major theoretical and experimental debate on the influence of the excited Cl* in the reactivity of the Cl + H_2 reaction. Different laboratories (Alexander, Werner, Neumark, Cassavechia, and their coworkers) [62–67] performed theoretical/experimental studies of the validity of the BO approximation in this reaction, concluding that the adiabatically allowed reaction [$Cl(^2P_{3/2})+H_2$] will dominate the adiabatically forbidden reaction [$Cl(^2P_{1/2})+H_2$]. Hence, these results are in direct contrast with the experiment of Liu et al. [59–61], suggesting that this experiment claiming high reactivity of Cl* needs to be re-examined.

In the case of the NH_3+Cl reaction, we suppose a similar behaviour, where the role of the excited Cl* state will be negligible or minor.

Another important property is the equilibrium constant (K_{eq}). It is calculated in the transition-state theory approach based only on reactant and product properties, and hence, the reaction path properties cancel out. Table VI lists the K_{eq} values in the temperature range 298–2000 K together with values obtained from thermochemical calculations,

$$K_{eq} = \exp\left(-\frac{\Delta H_R^o}{RT} + \frac{\Delta S_R^o}{R}\right) \tag{10}$$

where ΔH_R^o and ΔS_R^o are, respectively, the enthalpy and the entropy of reaction. Two series of thermochemical data have been published: the JANAF tables [32] and Gao et al. [24] who proposed the expression $k_{eq} = 27.3 \times T^{-0.049}$ exp(−2248/T) over 200–2000 K based on their experimental enthalpies of reaction and tabulated data [68]. These two series show major discrepancies, especially at low temperatures. Our results are in excellent agreement with the values reported by Gao et al. [24], which seems to indicate that the JANAF values are underestimated at low temperatures. This difference could be explained by taking into account that the K_{eq} value obtained from thermochemical data depends on the standard enthalpy of reaction,

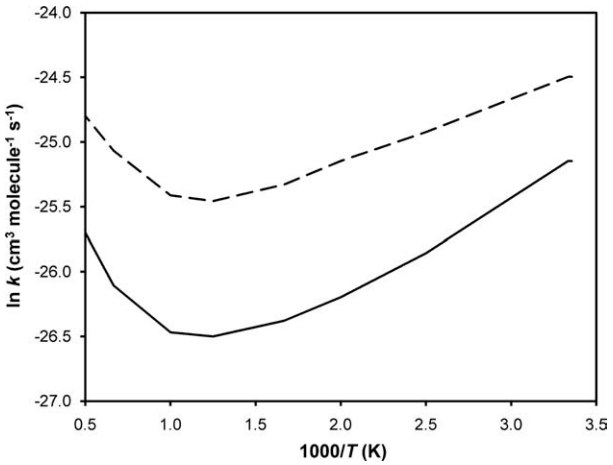

FIGURE 8. Arrhenius plots of ln k (cm^3 $molecule^{-1}$ s^{-1}) for the reverse thermal rate constants against the reciprocal of temperature (K) in the range 300–2000 K. Solid line: PES-2010; dashed line: theoretical values from Ref. [24].

ΔH^{o}_{R}, which can be obtained from the corresponding standard enthalpies of formation, $\Delta H^{o}_{f,i}$, of reactants and products. Although the ΔH^{o}_{f} values of NH_3, Cl, and HCl are well established [32], the proposed experimental values of the enthalpy of formation of the NH_2 free radical present discrepancies. In particular, they vary between 44.0 ± 2.3 (Ref. [69]) and 48.1 ± 3.5 (Ref. [70]) kcal mol^{-1}, although the latest compilations reduce this range. Thus, for instance, the JANAF tables [32] recommend 45.5 ± 1.5 kcal mol^{-1}, which agrees with a recent experimental determination [71]. However, recent theoretical [72] and experimental [73] studies reduce this value by one unit to 44.6 ± 0.1 and 44.5 ± 0.1 kcal mol^{-1}, respectively, which agree with our theoretical value [74] of 43.8 ± 0.6 kcal mol^{-1} within the uncertainties. Therefore, although the value of the enthalpy of formation of the NH_2 product seems still to be an open question, it doubtless strongly influences the standard enthalpy of reaction and hence the equilibrium constants, Eq. (10). For instance, a decrease of 1 kcal mol^{-1} increases K_{eq} by a factor of from ≈5 at 400 K down to ≈2 at 1000 K.

The equilibrium constants permit one to derive the reverse rate constants, k_r, NH_2 +HCl → NH_3 +Cl, taking into account the relationship $K_{eq} = k_f/k_r$. The PES-2010 reverse rate constants are listed in Table VI for the temperature range 298–2000 K, together with other published theoretical values [24] for comparison. The corresponding Arrhenius plots are shown in Figure 8. The two theoretical results have similar behavior, that is, a negative temperature dependence in the 300–1000 K range, changing to positive dependence in the higher temperature range, 1000–2000 K. Unfortunately, there are no experimental data available for comparison.

To understand the behavior of the activation energy, we analyzed the evolution of the variational transition states as a function of the temperature, where the activation enthalpy contribution is given by the expression

$$\Delta H^{*} = \mathrm{RT}^2 \frac{d \ln k}{dT} - 2\mathrm{RT} \tag{11}$$

In practice, the derivative in Eq. (11) is calculated by a two-point central difference algorithm.

At this point, it is useful to consider the following relationship between activation energy and the enthalpy change corresponding to the variational transition state,

$$E_a = \Delta H^{\mathrm{CVT,T}} + 2\mathrm{RT} \tag{12}$$

which holds for bimolecular reactions in the gas phase (provided that no tunneling effect exists). The contributions of $\Delta H^{\mathrm{CVT,T}}$ and 2RT as functions of temperature are plotted in Figure 9 together with their sum, that is, the activation energy. For the NH_2 + HCl reverse hydrogen abstraction reaction, the value of E_a depends on the balance between the 2RT term (which is always positive) and the $\Delta H^{\mathrm{CVT,T}}$ term (which is

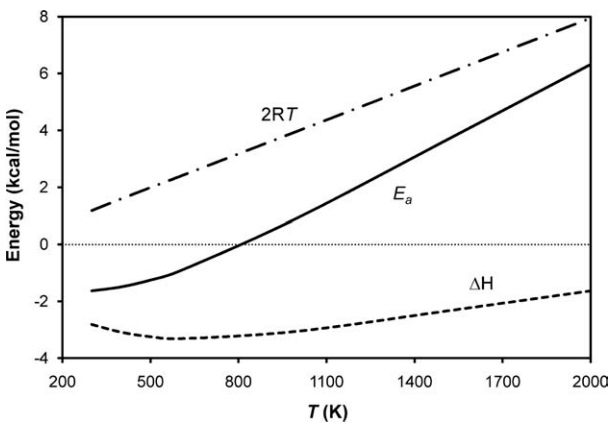

FIGURE 9. Activation energy profile and its enthalpic and 2RT contributions as a function of temperature over the 300–2000 K range for the reverse reaction. All values are taken versus products.

always negative in the range 298–2000 K). At high temperatures, $T > 800$ K, the 2RT term surpasses the negative $\Delta H^{CVT,T}$ term, and the activation energy becomes positive. With decreasing temperature, the negative $\Delta H^{CVT,T}$ term becomes large enough in absolute value to overcome the positive 2RT term and gives a negative activation energy.

Taking as reference the products, NH_2 + HCl, the reverse presents a reactive complex in the entry channel, CP, stabilized by 7.1 kcal mol^{-1} with respect to the products (Fig. 2). It is the existence of this intermediate complex, which is responsible for the observed negative temperature dependence at low temperatures.

7. Conclusions

We have described for the first time the construction of a new analytical PES for the hydrogen abstraction channel of the reaction between chlorine and ammonia, which presents various maxima and minima. The method was based on an analytical form developed by our research group, and the input information used for the fit was exclusively based on very high-level ab initio single point calculations, CCSD(T) = FULL/aug-cc-pVTZ.

First, the new surface, named PES-2010, was subjected to stringent tests against the ab initio information: geometries, vibrational frequencies and energies of the stationary points, topology of the reaction path, and the reaction swath. In general, bearing in mind the very complicated potential of this reaction with its various maxima and minima, these ab initio data used for the fit are reproduced well by the new PES, showing the validity of the fitting procedure. The main differences are the geometries of the wells and the bending angle at the saddle point. This latter is not collinear at the ab initio level, while the surface predicts a collinear structure. However, we showed that this limitation has no influence on the final kinetics results.

Second, as an additional test, the results of thermochemical (equilibrium constants, K_{eq}) and kinetics (thermal forward and reverse rate constants, k_f and k_r, and KIEs) calculations at the CCSD(T) = FULL/aug-cc-pVTZ single point level are reproduced by the analytical PES, showing the negligible influence of the tunneling effect for this reaction. This agreement is encouraging, because these properties were not included in the fit.

Third, as a first application of the use of the new PES, a kinetics study using variational transition-state theory was performed over the temperature range 200–2000 K. The forward thermal rate constants reproduce the sparse experimental information over the common temperature range. In the VTST approach, the reverse rate constant is obtained from the forward one by detailed balance, based on the equilibrium constant, K_{eq}, which depends only on reactant and product properties while the reaction path properties cancel out. Unfortunately, there are no experimental data available for comparison, but our results reproduce the behavior obtained in previous theoretical studies, that is, the change of the activation energy with temperature due to the presence of an intermediate complex in the exit channel.

In sum, for a surface as complicated as the present case, with several maxima and minima, the agreement obtained with the available thermochemical and kinetics measurements lends confidence to the new PES-2010 surface.

References

1. Ramachandran, C. N.; De Fazio, D.; Cavalli, S.; Tarantelli, F.; Aquilanti, V. Chem Phys Lett 2009, 469, 26.
2. George, F.; Sanjay, D. X. Chem Phys 2010, 373, 170.
3. Tanaka, T.; Takayanagi, T. Chem Phys Lett 2010, 496, 248.
4. Corchado, J. C.; Espinosa-Garcia, J. J Chem Phys 1997, 106, 4013.
5. Espinosa-Garcia, J.; Corchado, J. C. J Phys Chem A 1997, 101, 7336.
6. Espinosa-Garcia, J.; Corchado, J. C. J Phys Chem A 2010, 114, 4455.
7. Espinosa-Garcia, J.; Corchado, J. C. J Chem Phys 1996, 100, 16561.
8. Espinosa-Garcia, J. J Chem Phys 2002, 116, 10664.
9. Corchado, J. C.; Bravo, J. L.; Espinosa-Garcia, J. J Chem Phys. 2009, 130, 184314.
10. Espinosa-Garcia, J.; Sanson, J.; Corchado, J. C. J Chem Phys 1998, 109, 466.
11. J. Espinosa-Garcia, J. J Chem Phys 1999, 111, 9330.
12. Corchado, J. C.; Espinosa-Garcia, J. J Chem Phys 1996, 105, 3152.
13. Rangel, C.; Navarrete, M.; Espinosa-Garcia, J. J Phys Chem A 2005, 109, 1441.
14. Espinosa-Garcia, J.; Bravo, J.L.; Rangel, C. J Phys Chem A 2007, 111, 2761.

15. Espinosa-García, J.; Corchado, J. C. J Chem Phys 1996, 105, 3517.
16. Corchado, J. C.; Truhlar, D. G.; Espinosa-García, J. J Chem Phys 2000, 112, 9375.
17. Rangel, C.; Navarrete, M.; Corchado, J. C.; Espinosa-Garcia, J. J Chem Phys 2006, 124, 124306.
18. Espinosa-García, J.; Corchado, J. C. J Chem Phys 2000, 112, 5731.
19. Rangel, C.; Espinosa-Garcia, J. J Phys Chem A 2006, 110, 537.
20. Rangel, C.; Espinosa-Garcia, J. J Phys Chem A 2007, 111, 5057.
21. Clary, D.C. PNAS 2008, 105, 12649.
22. Miller, J. A.; Bowman, C. T. Prog Energy Combust Sci 1989, 15, 287.
23. Westenberg, A. A.; DeHaas, N. J Chem Phys 1977, 67, 2388.
24. Gao, Y.; Alecu, I. M.; Hsieh, P.-C.; Morgan, B. P.; Marshall, P.; Krasnoperov, L. N. J Phys Chem A 2006, 110, 6844.
25. Kondo, S.; Tokuhashi, K.; Kaise, M. J Hazard Mat A 2000, 79, 77.
26. Xu, Z. F.; Lin, M. C. J Phys Chem A 2007, 111, 584.
27. Monge-Palacios, M.; Espinosa-Garcia, J. J Phys Chem A 2010, 114, 4418.
28. Baldridge, K. M.; Gordon, M. S.; Steckler, R.; Truhlar, D. G. J Phys Chem 1989, 93, 5107.
29. Zhao, Y.; Truhlar, D. G. J Phys Chem A 2004, 108, 6908.
30. Bartlett, R. J. J Phys Chem 1989, 93, 1697.
31. Kendall, R. A.; Dunning, T. H.; Harrison, R. J. J Chem Phys 1992, 96, 6796.
32. Chase, M. W.; Davis, C. A., Downey, J. R.; Frurip, D. J.; McDonald, R. A.; Syverud, A. N. J Phys Chem Ref Data 1985, 14 (Suppl), 1.
33. Truhlar, D. G. Chem Phys Lett 1998, 294, 45.
34. Fast, P. L.; Sánchez, M. L.; Truhlar, D. G. J Chem Phys 1999, 111, 2921.
35. Zheng, J.; Zhao, Y.; Truhlar, D. G. J Chem Theory Comput 2009, 5, 808.
36. Frisch, M. J.; Trucks, G. W.; Schlegel, H. B.; Scuseria, G. E.; Robb, M. A.; Cheeseman, J. R.; Zakrzewski, V. G.; Montgomery, J. A.; Stratman, R. E.; Burant, J. C.; Dapprich, M.; Millam, J. M.; Daniels, A. D.; Kudin, K. N.; Strain, M. C.; Farkas, O.; Tomasi, J.; Barone, V.; Cossi, M.; Cammi, R.; Menucci, B.; Pomelli, C.; Adamo, C.; Clifford, S.; Ochterki, J.; Petterson, G. A.; Ayala, P. Y.; Cui, Q.; Morokuma, K.; Malik, D. K.; Rabuk, A. D.; Raghavachari, K.; Foresman, J. B.; Cioslowski, J.; Ortiz, J. V.; Stefanov, J. J.; Liu, G.; Liashenko, A.; Piskorz, P.; Komaromi, I.; Gomperts, R.; Martin, R. L.; Fox, D. J.; Keith, T.; Al-Laham, M. A.; Peng, C. Y.; Nanayakkara, A.; González, C.; Challacombe, M.; Gill, P. M. W.; Johnson, B. G.; Chen, W.; Wong, M. W.; Andres, J. L.; Head-Gordon, M.; Reploge, E. S.; Pople, J. A. Gaussian 03 program, Revision B.05; Gaussian Inc.: Pittsburg, PA, 2003.
37. (a) London, F. Probleme der Modernen Physik Sommerfeld–Festschrift, S. Hirzel Leipzig, 1928, 104; (b) Eyring, H.; Polanyi, M. Z Phys Chem 1931, 1312, 279.
38. Chakraborty, A.; Zao, Y.; Lin, H.; Truhlar, D. G. J Chem Phys 2006, 124, 044315.
39. Espinosa-Garcia, J. J Phys Chem A 2001, 105, 134.
40. Espinosa-Garcia, J. J Phys Chem A 2001, 105, 8748.
41. Page, M.; McIver, J. W. J Chem Phys 1988, 88, 922.
42. Fast, P. L.; Truhlar, D. G. J Chem Phys 1988, 109, 3721.
43. Jackels, C. F.; Gu, Z.; Truhlar, D. G. J Chem Phys 1995, 102, 3188.
44. Chuang, Y.-Y.; Truhlar, D. G. J Phys Chem A 1998, 102, 242.
45. Garrett, B. C.; Truhlar, D. G. J Am Chem Soc 1979, 101, 4534.
46. Truhlar, D. G.; Isaacson, A. D.; Garrett, B. C. In Theory of Chemical Reaction Dynamics; Baer, M., Eds.; Chemical Rubber: Boca Raton, FL, 1985; Vol. 4, p65.
47. Corchado, J. C.; Chuang, Y.-Y.; Fast, P. L.; Hu, W.-P.; Liu, Y.-P.; Lynch, G. C.; Nguyen, K. A.; Jackels, C. F.; Fernandez-Ramos, A.; Ellingson, B. A.; Lynch, B. J.; Melissas, V. S.; Villà, J.; Rossi, I.; Coitiño, E. L.; Pu, J.; Albu, T.; Steckler, R.; Garrett, B. C.; Isaacson, A. D.; Truhlar, D. G. Polyrate 9.5.; University of Minnesota: Minneapolis, 2007.
48. Liu, Y.-P.; Lynch, G. C.; Truong, T. N.; Lu, D.-H.; Truhlar, D. G. J Am Chem Soc 1993, 115, 2408.
49. Fernandez-Ramos, A.; Truhlar, D. G. J Chem Phys 2001, 114, 1491.
50. Garrett, B. C.; Truhlar, D. G. J Chem Phys 1983, 79, 4931.
51. Meana-Pañeda, R.; Truhlar, D. G.; Fernandez-Ramos, A. J Chem Theory Comput 2010, 6, 6.
52. Fast, P. L.; Corchado, J. C.; Truhlar, D. G. J Chem Phys 1998, 109, 6237.
53. Espinosa-García, J.; Corchado, J. C. J Chem Phys 1994, 101, 1333.
54. Meuwly, M.; Hutson, J. M. J Chem Phys 2000, 112, 592.
55. Meuwly, M.; Hutson, J. M. Phys Chem Chem Phys 2000, 2, 441.
56. Zdanska, P.; Nachtigallova, D.; Nachtigall, P.; Jungwirth, P. J Chem Phys 2001, 115, 5974.
57. Klos, J.; Szczesniak, M. M.; Chalasinski, G. Int Rev Phys Chem 2004, 23, 541.
58. Merritt, J. M.; Küpper, J.; Miller, R. E. Phys Chem Chem Phys 2007, 9, 401.
59. Lee, S.-H.; Lai, L.-H.; Liu, K.; Chang, H. J Chem Phys 1999, 110, 8229.
60. Lee, S.-H.; Liu, K. J Chem Phys 1999, 111, 6253.
61. Dong, F.; Lee, S.-H.; Liu, K. J Chem Phys 2001, 115, 1197.
62. Alexander, M. H.; Capecchi, G.; Werner, H.-J. Science 2002, 296, 715.
63. Balucani, N.; Skouteris, D.; Cartechini, L.; Capozza, G.; Segoloni, E.; Casavecchia, P.; Alexander, M. H.; Capecchi, G.; Werner, H.-J. Phys Rev Lett 2003, 91, 013201.
64. Alexander, M. H.; Capecchi, G.; Werner, H.-J. Faraday Discov 2004, 127, 59.
65. Garand, E.; Zhou, J.; Manolopoulus, D. E.; Alexander, M. H.; Neumark, D. M. Science 2008, 319, 72.
66. Neumark, D. M. J Phys Chem A 2008, 112, 13287.
67. Wang, X.; Dong, W.; Xiao, Ch.; Che, L.; Ren, Z.; Dai, D.; Wang, X.; Casavecchia, P.; Yang, X.; Jiang, B.; Xie, D.; Sun, Z.; Lee, S-Y.; Zhang, D. H.; Werner, H.-J.; Alexander, M. H. Science 2008, 322, 573.

68. Gurvich, L. V.; Veyts, I. V.; Alcock, C. B. Eds. Thermodynamic Properties of Individual Substances, 4th Ed.; Hemisphere: New York, 1989; Vol. 1.
69. Defrees, D. J.; Hehre, W. J.; McIver, R. T.; McDanile, D. H. J Phys Chem 1979, 83, 232.
70. Carson, A. S.; Laye, P. G.; Yurekli, M. J Chem Thermodyn 1977, 9, 827.
71. Friedrichs, G.; Wagner, H. G. Z Phys Chem 2000, 214, 1151.
72. Dixon, D. A.; Feller, D.; Peterson, K. A. J Chem Phys 2001, 115, 2576.
73. Song, Y.; Qian, X.-M.; Lan, K. C.; Ng, Y. C.; Liu, J.; Chen, W. J Chem Phys 2001, 115, 2582.
74. Espinosa-Garcia, J.; Corchado, J. C.; Marquez, A. Chem Phys Lett 1995, 233, 220.